Multiclass Diabetic Retinopathy: Hybrid Metaheuristic Particle Swarm Optimization and Classification for Severity Grading and Feature Extraction

Asif Raza
Malaysian Institute of Information Technology, Universiti Kuala Lumpur, Malaysia | Sir Syed University of Engineering and Technology, Karachi, Pakistan
asif.raza@ssuet.edu.pk

Shahrulniza Musa
Malaysian Institute of Information Technology, Universiti Kuala Lumpur, Malaysia
shahrulniza@unikl.edu.my (corresponding author)

Ahmad Shahrafidz Khalid
Malaysian Institute of Information Technology, Universiti Kuala Lumpur, Malaysia
ahmads@unikl.edu.my

Muhammad Mansoor Alam
Faculty of Computing and Informatics, Multimedia University, Cyberjaya, Malaysia
mansoor@mmu.edu.my

Mazliham Mohd Su'ud
Faculty of Computing and Informatics, Multimedia University, Cyberjaya, Malaysia
mazliham@mmu.edu.my

Fouzia Noor
Department of Diagnostic and Radiology, Combined Military Hospital, Karachi, Pakistan
drfouzianoor123@gmail.com

Received: 26 March 2025 | Revised: 27 April 2025, 8 May 2025, and 13 May 2025 | Accepted: 15 May 2025

 DOI: https://doi.org/10.48084/etasr.11147

ABSTRACT

This study aimed to effectively classify a Diabetic Retinopathy (DR) image dataset consisting of colored images by developing a hybrid and robust transfer learning model called MOB-PSO, integrating MobileNet with Particle Swarm Optimization (PSO) to enhance performance and accuracy. A well-structured dataset is crucial for building a high-performance model capable of accurate feature extraction and precise identification of image features within each class. Traditional statistical algorithms often struggle to classify colored images accurately, leading to errors in detecting diseases within DR image datasets. To reduce error rates and improve classification accuracy, this study developed a hybrid, reliable, and optimized image classification model. The DR dataset consists of ten distinct classes. Experimental results demonstrate that the MOB-PSO model surpasses state-of-the-art algorithms in terms of accuracy, robustness, precision, recall, and F1 score, achieving optimal validation loss values. Specifically, the MOB-PSO model recorded training and validation losses of 0.1515 and 0.1853, respectively, with corresponding accuracies of 98.58% and 96.7%. The precision, recall, and F1-score were 0.9744, 0.9657, and 0.9698, respectively, showcasing the model's effectiveness.

Keywords-MobileNet; CNN; deep learning; diabetic retinopathy; Particle Swarm Optimization (PSO)

I. INTRODUCTION

In recent years, Deep Learning (DL) has outperformed traditional machine learning techniques in several fields, most notably in computer vision. Convolutional Neural Networks (CNNs), Deep Boltzmann Machines (DBMs), Deep Belief Networks (DBNs), and Stacked Denoising Autoencoders (SDAs) are among the crucial DL techniques for computer vision tasks [1].

In [2], scale and orientation-selective Gabor filter series were used to automatically detect and classify vascular abnormalities that are related to Diabetic Retinopathy (DR), successfully identifying abnormalities. The field of automatic medical image analysis has expanded rapidly and expanded significantly in recent years [3, 4]. The advent of CNN architectures, which have demonstrated remarkable predictive power and have reached the same level of performance as clinicians, is used as one of the main driving forces behind the emergence of the trend [5]. The ultimate goal is for health professionals to use the models as clinical decision-support tools that should provide high diagnostic accuracy [6]. These techniques consist of two primary segmentation stages: fine segmentation using morphological reconstruction and coarse segmentation using fuzzy C-Means clustering [7].

In DR, the blood vessels and layers of the retina are affected. Early detection is important, but the high cost of current diagnostic techniques makes it difficult. In [8], traditional DR detection methods were described. Labor-intensive retinal image grading is a time-consuming, inaccurate, and inconvenient process for patients. In [9], a hybrid network combined DenseNet121, VGG16, and the XGBoost classifier to detect and classify DR. In [10], a mathematical method was proposed, which incorporates feature selection, subset reduction, and feature extraction into its preprocessing approach, removing the need for additional techniques to expand datasets without sacrificing efficacy.

The main contributions of this paper can be summarized as:

- Introduces an improved metaheuristic dual deterministic model (Mobile Net + PSO) for feature extraction and DR classification. The MobileNet model is further integrated and optimized with a metaheuristic Particle Swarm Optimization algorithm.
- Using MOB-PSO, an objective function represents and updates a particle's position in a swarm with a user-defined learning rate.
- The main advantage is the introduction of two straightforward global hyperparameters, width and resolution, that efficiently balance delay, improve accuracy, and lower error rate. Based on particular problem constraints, the model builder can select the ideal model size for these hyperparameters.
- This study used data that was ethically approved by the Unikl Research Ethics Committee.

Multimodal Optimization Problems (MMOPs) are used as novel optimization techniques which are known as Memetic Direction Exploitation (MDE). In [11, 12], classification methods for DR using CNN were optimized using PSO. Fine-tuning is a key technique in CNN parameters, such as the number of convolutional layers, filter size, and pooling layers. In [13], the Gray Level Run Length Matrix (GLRLM) and feature extraction were used to detect and classify DR. To determine and evaluate the most accurate detection method, each classifier was tested using a texture feature technique. In [14], P-EDR used image processing to identify the disease by extracting features such as hemorrhages from NPDR retina images. P-EDR is an effective model for more accurately diagnosing DR because it uses important features for detection and classification. In [15], an automated DR detection method used retinal fundus images and the Glowworm Swarm Optimization (GSO) with Deep Learning (ADR-GSODL). This was achieved by enforcing Median Filtering (MF) as a pre-processing step in the ADR-GSODL method. In [16], an innovative approach was proposed to classify exudates in fundus images. Preserving important features using a feature vector technique, fundus images were resized using image augmentation.

II. METHODOLOGY

A. Dataset Details and Preprocessing

As shown in Table I, the dataset was divided into three subsets for training, validation, and testing. MobileNet is structured into blocks, and the training process ensures accurate outputs. The images were resized to a standard dimension of 224×224. A batch size of 256 was applied to rescale pixel values, normalizing the data within a 0-1 range for improved processing efficiency. For the simulation process, every DR image was converted into a JPEG format, which was originally annotated by medical practitioners. Every image has a resolution of 72 dpi, with a file size of 2.01 MB. Each image's original resolution was 2976×2976 dpi on both axes, with a bit depth of 24.

TABLE I. SIMULATION PROCESS

	Number of images
Training set	3790
Test set	1525
Validation set	1505

TABLE II. IMAGES PER CLASS

DR classes	**Images**	**Training (70%)**	**Validation (15%)**	**Testing (15%)**
Diabetic Papillopathy	825	459	183	183
Mild NPDR	813	451	173	189
Mild NPDR+CSME	1287	717	287	283
Moderate NPDR	862	481	188	193
Moderate NPDR +CSME	424	238	95	91
PDR+CSME	157	87	33	37
PDR	1213	670	277	266
Severe NPDR	129	70	29	30
Severe NPDR+CSME	579	321	127	131
Very Severe NPDR	531	296	113	122
Total		**3790**	**1505**	**1525**

B. Optimizing Hybrid Particle Swarms for Multiclass OCT

MobileNet simplifies the conventional convolution process by using depth-wise separable convolutions, as shown in Figure 1. Its fundamental structure consists of batch normalization, ReLU activation, depth-wise convolutions, and 3×3 point-wise convolutions. The Width multiplier (W_m) evenly thins the network at each layer and the Resolution multiplier (R_m) lowers the input size and the internal representation of each layer. These are two parameters that MobileNet uses to balance delay and accuracy. The computation (M_c) for the core layers is expressed in (1), depending on the feature map size $F_D \times F_D$, kernel size $K_D \times K_D$, input channels M, and output channels N_C.

$$M_C = K_D \cdot K_D \cdot W_m.M \cdot R_m.F_D \cdot R_m.F_D + W_m.M \cdot W_m.N_C \cdot R_m.F_D \cdot R_m.F_D \quad (1)$$

where $K_D \cdot W_m.M \cdot R_m \cdot F_D$ and $W_m \cdot N$ are variables or parameters. The (·) symbol represents multiplication.

In identifying DR classes, W_m and R_m are set to 1. Under these conditions, the computational cost of the Standard Convolution can be determined using:

$$StandardConv = K_D \cdot K_D \cdot N_C.M \cdot F_D.F_D \quad (2)$$

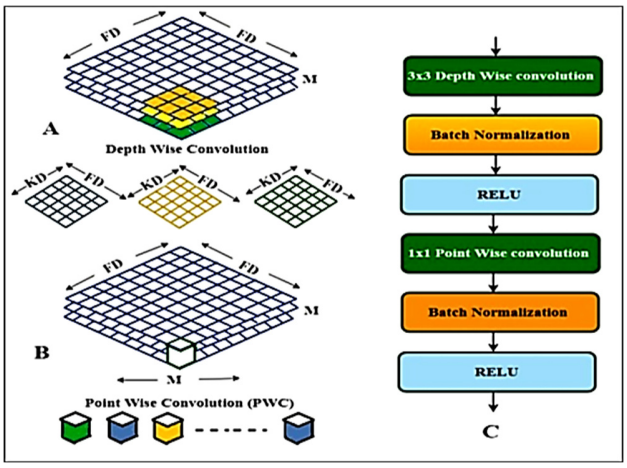

Fig. 1. MobileNet layer architecture and normalization.

$$R = \frac{Wm.Rm^2}{Nc} + \frac{Wm^2.Rm^2}{\mathrm{D}^2k} \quad (3)$$

The two simple global hyperparameters, resolution and width multipliers, are the main advantages of the suggested model. The ideal model size that was adapted to particular problem constraints was made possible by these parameters' successful ability to balance the delay, accuracy, and loss.

PSO is a random optimization technique inspired by the natural behavior of swarms [17]. PSO starts with a swarm of particles, each representing a random practical solution with an assigned random velocity, moving through the search space. The particles are guided toward the optimal solution based on the best fitness achieved by any particle in the swarm. The PSO update rule has various adjustable elements (4). Table III shows the parameters of the objective function.

$$v_i(t+1) = v_i(t) + .r_1.\{pbest_i - x_i(t)\} + c_2.r_2.\{gbest_i - x_i(t)\} \quad (4)$$

TABLE III. PARAMETERS

Parameters	Values
Swarm size	2
Learning rate	x[0]
Num_Epochs (Number of epochs)	round(x[1])
Max_Epochs (Maximum Epochs)	2
w (Inertia weight)	0.8
c1, c2 (Cognitive coefficient, Social coefficient)	1,1.2
Max_iter (Maximum number of iterations)	02
Lower and upper bounds and number of epochs	[0.001, 5], [0.005, 6]

Convolutions generate feature maps by applying learnable filters to each layer's input. This is a methodical approach to combining two disparate images, after which a function assumes a new shape. This is a basic function of CNNs and has been used traditionally in image processing for blurring, sharpening, detecting edges, and embossing images. The feature map $\{F_{map}^{lr}(a,b,n)\}$ for neuron n in layer lr can be computed as:

$$F_{map}^{lr}(a,b,n) = B_n^{lr} + X^{lr-1}(a,b,c) * K_n^{lr}(a,b,c) \quad (5)$$

where X^{lr-1} is the input from the preceding layer. The value of the input unit within channel c is represented by each element (a,b,c), where a and b are rows and columns, respectively. The number of channels in the current layer is the same as that of X^{lr-1}. The corresponding biases B_n^{lr}. are then added to the convolved feature maps in a particular layer. A dense layer contains 1024 units [18]. The activations of every extracted convolved feature are calculated using a non-linear activation function, ReLU. In both the convolutional and fully connected layers, ReLU is commonly applied to the output of every hidden unit [19]. The output of $ReLU^{lr}(a,b,n)$ is given by:

$$ReLU^{lr}(a,b,n) = max\left(0, {F_{map}}^{lr}(a,b,n)\right) \quad (6)$$

Local Response Normalization (LRN) is used to add generalization and non-linearity to the ReLU response. Considering the activity of nearby neurons, this extra element improves performance in terms of model accuracy and stability. LRN is calculated is given by:

$$Norm^{lr}(a,b,n) = ReLU^{lr}(a,b,n) (\alpha + \gamma \sum_{j \in Ml} (R^{lr}(a,b,j))^2)^{-\beta} \quad (7)$$

The ReLU output is passed through $Norm^{lr}(a,b,n)$. Each ReLU output in layer lr is multiplied by the inverse of the sum of squares by a counterweight γ.

C. Back Propagation and Weights Declaration

The gradient computation method is frequently used in neural network training [20]. However, its implementation on edge devices may necessitate significantly more hardware and software resources than those in the central location. A simplified expression of the weight update for a single weight w in a neural network using gradient descent optimization is:

$$w_{\{t+1\}} = w_{\{t\}} - \alpha \cdot \frac{\partial L}{\partial w} \quad (8)$$

D. Stochastic Gradient Descent (SGD)

SGD is a straightforward and efficient method that determines the gradient of the loss function for the weights of the neural network and then modifies them to decrease the loss function [21]. As stated in (9), consider a neural network with a single weight w and a squared error loss function L:

$$L = \frac{1}{2}(y_{true} - y_{Pred})^2 \quad (9)$$

where y_{true} is the true target output, and y_{Pred} represents the predicted output of the neural network.

$$\frac{\partial L}{\partial w} = \frac{\partial L}{\partial y_{Pred}} * \frac{\partial y_{Pred}}{\partial w} \quad (10)$$

E. Flatten Layer Customization

This layer is used to flatten the base CNN model's output, which includes features that were taken from the input image [22]. This multi-dimensional tensor is transformed into a one-dimensional array by the flatten layer so that it can be used as input for further processes. Usually, a feature vector results in a flattened array in feature extraction. Suppose an input tensor X that has the following dimensions Q, Ch, He, and Wi. He is the height of the processed data, Wi is its width (feature map), Q is the amount of data processed in a single iteration, and Ch is the number of channels used to store data. The input tensor X is converted into a one-dimensional array, denoted as (Q, M), where $(M = Ch * He * Wi)$, by the flatten operation.

$$X'(Q, m) = X(Q, Ch, He, Wi) \quad (11)$$

This type of regularization, as explained in [22], is employed to stop neural networks from overfitting. It operates by randomly removing certain neurons based on the dropout rate during training, enforcing generalization and robustness. To improve feature extraction, a dropout layer was added right after the dense layer. In each training iteration, 20% of the neurons in the dense layer are randomly removed, a process known as dropout. The subset D of neurons is chosen at random to be dropped during the training given input X, where $D \subseteq \{1, 2, \dots, n\}$ and the dropout rate is $| D |= p \cdot n$. The output of (12) is obtained when dropout is not used during inference (testing and prediction).

$$y = (1 - p) \cdot x \quad (12)$$

To compensate for the neurons that are omitted during training, the dropout layer adjusts the output by a factor of $\frac{1}{1-p}$. During inference, to maintain the expected output magnitude, the output is instead scaled by $(1 - p)$.

III. RESULTS

Performance metrics per class were used to evaluate the different stages of DR, as shown in Table III. In Diabetic Papillopathy, the model correctly identified 175 true positives and 1319 true negatives, with only 3 false positives and 8 false negatives. In Mild NPDR+CSME, the model achieved somewhat higher precision and recall than in Mild NPDR. The F1-score for Moderate NPDR was 0.976 due to its remarkable recall of 0.984 and precision of 0.969. For Moderate NPDR+CSME, the model accurately identified 92 true positives and 1409 true negatives, with only 1 false positive and 3 false negatives. In PDR+CSME, an F1-score of 93.75% was achieved, as the model identified 30 true positives, 1 false positive, 3 false negatives, and 1471 true negatives. In PDR, a precision of 97.17% was achieved. For Severe NPDR, the model demonstrated its strong performance by correctly identifying 29 true positives and avoiding false positives or negatives. Similar results were achieved for Very Severe NPDR, correctly and error-free identifying all 113 true positives and 1392 true negatives. In all cases, the MOBPSO model produced accurate predictions.

TABLE IV. PERFORMANCE METRICS PER CLASS

Class	Precision	Recall	F1-score	TP	FP	TN	FN
Diabetic Papillopathy	0.9831	0.956	0.969	175	3	1319	8
Mild NPDR	0.9371	0.948	0.942	164	11	1321	9
Mild NPDR+CSME	0.962	0.972	0.967	279	11	1207	8
Moderate NPDR	0.969	0.984	0.976	185	6	1311	3
Moderate NPDR+CSME	0.989	0.968	0.979	92	1	1409	3
PDR+CSME	0.968	0.909	0.937	30	1	1471	3
PDR	0.972	0.993	0.982	275	8	1220	2
Severe NPDR	1.00	1.00	1.00	29	0	1476	0
Severe NPDR+CSME	0.967	0.929	0.948	118	4	1374	9
Very Severe NPDR	1.00	1.00	1.00	113	0	1392	0

Figure 2 demonstrates the robustness of the MOB-PSO model, which gradually improves with epochs. The model achieves a training accuracy of 75% and a validation accuracy of roughly 85% in the first iteration. The validation accuracy marginally exceeds 95%, surpassing the training accuracy of 90% in the second iteration. At the end of the third epoch, training accuracy approaches 98.58% and the validation accuracy falls just short of 96.7%. Training and validation accuracies are almost equal, indicating that the model is successfully learning from the data without overfitting. Both training and validation accuracies significantly improved over epochs, indicating that the model's capacity to generalize to unknown data has steadily improved with every iteration.

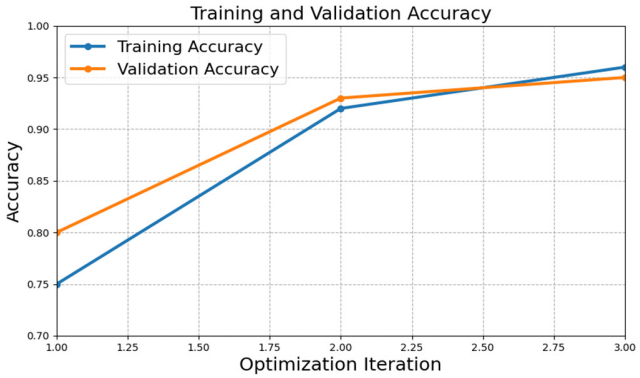

Fig. 2. Training and validation accuracy.

Figure 3 shows the training and validation loss across three epochs. The validation loss is lower in the first iteration, while the training loss starts higher and ends at 0.30. A well-generalizing model may achieve a good balance between its performance on the training and validation, as evidenced by the dropping toward zero loss. When both losses converge to certain values at the final iteration, this balance remains intact. In the third epoch, the validation loss is slightly higher than the training loss, which slides to 0 to 0.2, ensuring further optimization in error reduction.

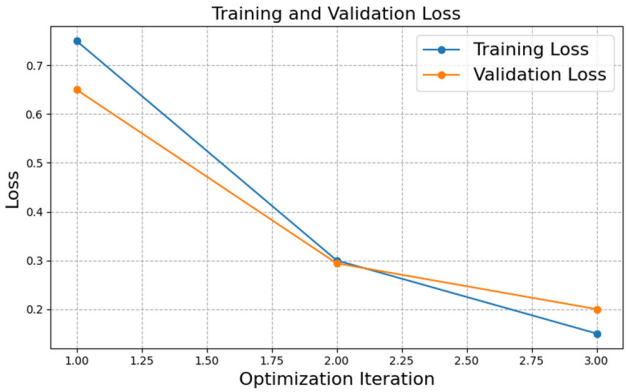

Fig. 3. Validation and training loss.

Figure 5 shows the number of images per class in the training dataset. With 717 images, Mild NPDR+CSME has the most images, followed by PDR with 670 images. Other classes with comparatively large image counts are Very Severe NPDR (296 images) and Mild NPDR (451 images). The PDR+CSME class had the fewest images (87). In addition, 238 images were Moderate NPDR+CSME and 70 were Severe NPDR.

Fig. 4. Image count (Training).

A. *Confusion Matrix on the Training and Validation Sets*

The model correctly identified 451 cases in the Diabetic Papillopathy class, but incorrectly identified 1 instance as Mild NPDR, 3 as Mild NPDR+CSME, 2 as Moderate NPDR, and 2 as Very Severe NPDR. The classification pattern represents no misclassifications for the Mild NPDR and Very Severe NPDR, showing that the model exhibits excellent accuracy with the least error rate. However, there were minor misclassifications in some classes, such as Severe NPDR+CSME, where a few cases were misclassified into adjacent classes, e.g., Mild NPDR+CSME, and 8 cases were misclassified as Diabetic Papillopathy. The few off-diagonal entries imply misclassifications between closely related DR processing stages, whereas the high numbers on the diagonal generally show strong model performance.

In the validation set, of the 182 images of Diabetic Papillopathy, 173 were correctly identified, while 10 were missed. There were 14 incorrect and 269 correctly classified images in Mild NPDR+CSME. With 190 correctly classified and 3 misclassifications, the model demonstrated high accuracy in Moderate NPDR. Four images were misclassified, and 87 were correctly classified as Moderate NPDR+CSME. The model correctly classified 35 images and misclassified 2 as PDR+CSME. There was only one misclassification out of 265 correctly classified images for PDR. In Severe NPDR, the model demonstrated perfect accuracy, correctly classifying all 30 images without any misclassifications. For Severe NPDR+CSME, there were 123 correctly classified images and 8 misclassified images. Finally, 122 images with Very Severe NPDR were correctly classified without any misclassifications.

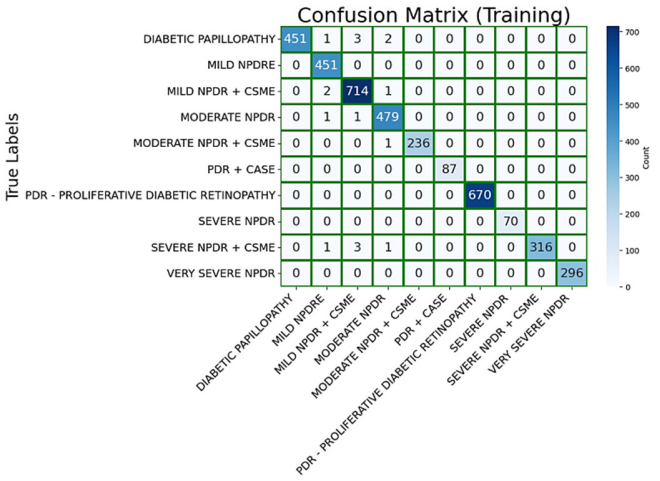

Fig. 5. Confusion matrix for training.

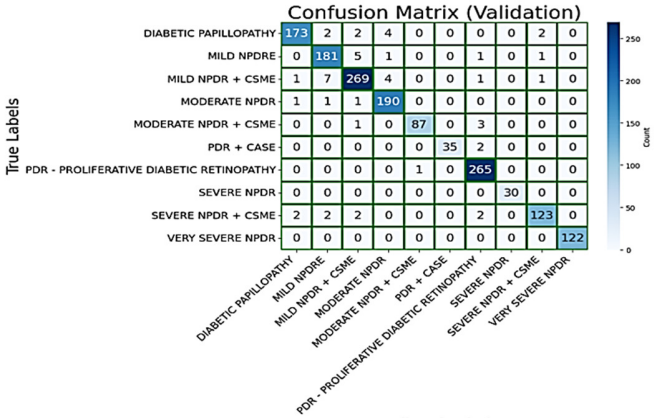

Fig. 6. Confusion matrix for the validation set.

B. Area Under the Receiver Operating Characteristic Curve (AUC)

Diabetic Papillopathy had an AUC of 1.00 and an accuracy of 0.96. Mild NPDR had an AUC of 0.99 and an accuracy of 0.95. Mild NPDR+CSME had an AUC of 1.00 and an accuracy of 0.97. PDR+CSME had an AUC of 1.00 and an accuracy of 0.91. PDR had an AUC of 1.00 and an accuracy of 0.99. Severe NPDR had an AUC of 1.00 and an accuracy of 0.00. Severe NPDR+CSME had an AUC of 1.00 and an accuracy of 0.93. Finally, Very Severe NPDR had an AUC of 1.00 and an accuracy of 1.00.

The following error rates were observed for each class: Diabetic Papillopathy: 0.02, Very Severe NPDR: 0.00, Severe NPDR+CSME: 0.03, Severe NPDR: 0.00, PDR: 0.03, PDR+CSME: 0.03, Moderate NPDR+CSME: 0.01, Moderate NPDR: 0.03, Mild NPDR+CSME: 0.04, Mild NPDR: 0.06, and Diabetic Papillopathy: 0.02.

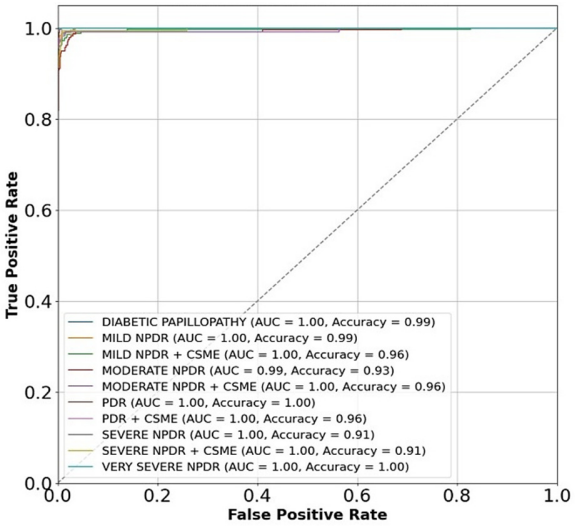

Fig. 7. ROC with error rate and class accuracy.

C. Model Comparision

Table V presents a comprehensive review of some studies in the field of DR classification, including the proposed model.

TABLE V. COMPARATIVE ANALYSIS

Ref.	Model	Dataset	Accuracy %
[23]	RNN-LSTM+CPSO	APTOS 2019	99.64
[24]	U-Net and sparse Fuzzy C-means+CTSA	DIARETDB1	95.9
[25]	ECNNs+HHO	IDRiD/Messidor	98
[26]	PSOSVM	APTOS-2019	93
[27]	ANNPSO	PIMA	94.15
[28]	SqueezeNet+PSo+CSA	Classic DR	96.8
[29]	HHO and GA	pvt	82.05
[30]	CFS+PSO	UCI Machine Repository	93.5
[31]	BFO+EPO	Public	96.55
Proposed	**MOB-PSO**	**Private**	**98.58**

IV. CONCLUSION AND FUTURE WORK

This research is extremely important for the urgent need to detect fundus and vision loss issues. The characteristics of blood vessels and other veins, which are finely layered inside the fundus and exhibit a high rate of variation in their volume, nature, and color contrast, make the classification of DR challenging. Since it can support both medical diagnosis and individualized treatment plans for patients with diabetes mellitus, accurate DR image classification has become increasingly significant in recent years. By utilizing DL capabilities, this study improves the detection, feature extraction, and classification of DR datasets using the Metaheuristic MOB-NET model. This study demonstrated the model's noteworthy effectiveness and resilience using a sizable dataset. The results showed that DL optimization methods are very effective and efficient in DR detection, feature extraction, and classification, achieving an accuracy of 98.58%. It is noteworthy that transfer learning led to notable performance gains, encouraging opportunities for better patient outcomes and a decline in the global incidence of visual impairments. Future work aims to use VGAN to improve the performance and robustness of the model.

DATA COLLECTION STATEMENT

This research was conducted at MIIT, University of Kuala Lumpur, Malaysia. The dataset used in this study was specifically gathered under approoval of the Research Ethics Committee (UNIKL REC/2024/PG/APV/01). The DR dataset used in this study was specifically collected for research and development purposes from the National Medical Center [32]. This dataset is not publicly available, but it can be provided upon reasonable request.

SIMULATION ENVIRONMENT

Anaconda 6.5 Python was used with an Intel Core i7-2720QM CPU at 2.4 GHz, Intel HD Graphics 6000, and 32 GB of RAM.

FUNDING STATEMENT

This work was supported by Universiti Kuala Lumpur under a Government Linked University (GLU) Grant with grant number GRCF2023_01.

REFERENCES

[1] A. Voulodimos, N. Doulamis, A. Doulamis, and E. Protopapadakis, "Deep Learning for Computer Vision: A Brief Review," *Computational Intelligence and Neuroscience*, vol. 2018, pp. 1–13, 2018, https://doi.org/10.1155/2018/7068349.

[2] D. Vallabha, R. Dorairaj, K. Namuduri, and H. Thompson, "Automated detection and classification of vascular abnormalities in diabetic retinopathy," in *Conference Record of the Thirty-Eighth Asilomar Conference on Signals, Systems and Computers, 2004.*, Pacific Grove, CA, USA, 2004, vol. 2, pp. 1625–1629, https://doi.org/10.1109/ACSSC.2004.1399432.

[3] G. Wang, "A Perspective on Deep Imaging," *IEEE Access*, vol. 4, pp. 8914–8924, 2016, https://doi.org/10.1109/ACCESS.2016.2624938.

[4] A. A. Siddique, A. Raza, M. S. Alshehri, N. Alasbali, and S. F. Abbasi, "Optimizing Tumor Classification Through Transfer Learning and Particle Swarm Optimization-Driven Feature Extraction," *IEEE Access*, vol. 12, pp. 85929–85939, 2024, https://doi.org/10.1109/ACCESS.2024.3412412.

[5] G. Litjens *et al.*, "A survey on deep learning in medical image analysis," *Medical Image Analysis*, vol. 42, pp. 60–88, Dec. 2017, https://doi.org/10.1016/j.media.2017.07.005.

[6] M. Puttagunta and S. Ravi, "Medical image analysis based on deep learning approach," *Multimedia Tools and Applications*, vol. 80, no. 16, pp. 24365–24398, Jul. 2021, https://doi.org/10.1007/s11042-021-10707-4.

[7] A. Sopharak and B. Uyyanonvara, "Automatic exudates detection from diabetic retinopathy retinal image using fuzzy c-means and morphological methods," in *Proceedings of the Third IASTED International Conference Advances in Computer Science and Technology*, 2007, pp. 359–364.

[8] P. Uppamma and S. Bhattacharya, "Deep Learning and Medical Image Processing Techniques for Diabetic Retinopathy: A Survey of Applications, Challenges, and Future Trends," *Journal of Healthcare Engineering*, vol. 2023, no. 1, Jan. 2023, Art. no. 2728719, https://doi.org/10.1155/2023/2728719.

[9] C. Mohanty *et al.*, "Using Deep Learning Architectures for Detection and Classification of Diabetic Retinopathy," *Sensors*, vol. 23, no. 12, Jun. 2023, Art. no. 5726, https://doi.org/10.3390/s23125726.

[10] F. H. Kuwil, "A new feature extraction approach of medical image based on data distribution skew," *Neuroscience Informatics*, vol. 2, no. 3, Sep. 2022, Art. no. 100097, https://doi.org/10.1016/j.neuri.2022.100097.

[11] S. Karthika and M. Durgadevi, "IMDE-UGAN: Improved Memetic Direction Exploitation Optimized U-Net Generative Adversarial Network for Classification of Diabetic Retinopathy," *IETE Journal of Research*, vol. 70, no. 8, pp. 6802–6818, Aug. 2024, https://doi.org/10.1080/03772063.2024.2310111.

[12] P. Melin, D. Sánchez, and R. Cordero-Martínez, "Particle Swarm Optimization of Convolutional Neural Networks for Diabetic Retinopathy Classification," in *Fuzzy Logic and Neural Networks for Hybrid Intelligent System Design*, vol. 1061, O. Castillo and P. Melin, Eds. Springer International Publishing, 2023, pp. 237–252.

[13] E. Barges and E. Thabet, "GLDM and Tamura features based KNN and particle swarm optimization for automatic diabetic retinopathy recognition system," *Multimedia Tools and Applications*, vol. 82, no. 1, pp. 271–295, Jan. 2023, https://doi.org/10.1007/s11042-022-13282-4.

[14] M. Hussain *et al.*, "An Enhanced Convolutional Neural Network (CNN) based P-EDR Mechanism for Diagnosis of Diabetic Retinopathy (DR) using Machine Learning," *Engineering, Technology & Applied Science Research*, vol. 15, no. 1, pp. 19062–19067, Feb. 2025, https://doi.org/10.48084/etasr.8854.

[15] R. Ramesh and S. Sathiamoorthy, "A Deep Learning Grading Classification of Diabetic Retinopathy on Retinal Fundus Images with Bio-inspired Optimization," *Engineering, Technology & Applied Science Research*, vol. 13, no. 4, pp. 11248–11252, Aug. 2023, https://doi.org/10.48084/etasr.6033.

[16] J. Ramya, M. P. Rajakumar, and B. U. Maheswari, "Deep CNN with Hybrid Binary Local Search and Particle Swarm Optimizer for Exudates Classification from Fundus Images," *Journal of Digital Imaging*, vol. 35, no. 1, pp. 56–67, Feb. 2022, https://doi.org/10.1007/s10278-021-00534-2.

[17] A. Raza, S. B. Musa, A. S. B. Khalid, M. M. Alam, M. M. Su'ud, and F. Noor, "Enhancing Medical Image Classification Through PSO-Optimized Dual Deterministic Approach and Robust Transfer Learning," *IEEE Access*, vol. 12, pp. 177144–177159, 2024, https://doi.org/10.1109/ACCESS.2024.3504266.

[18] A. M. Javid, S. Das, M. Skoglund, and S. Chatterjee, "A ReLU Dense Layer to Improve the Performance of Neural Networks," in *ICASSP 2021 - 2021 IEEE International Conference on Acoustics, Speech and Signal Processing (ICASSP)*, Toronto, Canada, Jun. 2021, pp. 2810–2814, https://doi.org/10.1109/ICASSP39728.2021.9414269.

[19] A. Krizhevsky, I. Sutskever, and G. E. Hinton, "ImageNet classification with deep convolutional neural networks," *Communications of the ACM*, vol. 60, no. 6, pp. 84–90, May 2017, https://doi.org/10.1145/3065386.

[20] A. Raza, M. S. Alshehri, S. Almakdi, A. A. Siddique, M. Alsulami, and M. Alhaisoni, "Enhancing brain tumor classification with transfer learning: Leveraging DenseNet121 for accurate and efficient detection," *International Journal of Imaging Systems and Technology*, vol. 34, no. 1, Jan. 2024, Art. no. e22957, https://doi.org/10.1002/ima.22957.

[21] Y. Tian, Y. Zhang, and H. Zhang, "Recent Advances in Stochastic Gradient Descent in Deep Learning," *Mathematics*, vol. 11, no. 3, Jan. 2023, Art. no. 682, https://doi.org/10.3390/math11030682.

[22] E. Jeczmionek and P. A. Kowalski, "Flattening Layer Pruning in Convolutional Neural Networks," *Symmetry*, vol. 13, no. 7, Jun. 2021, Art. no. 1147, https://doi.org/10.3390/sym13071147.

[23] Y. B. Özçelik and A. Altan, "Overcoming Nonlinear Dynamics in Diabetic Retinopathy Classification: A Robust AI-Based Model with Chaotic Swarm Intelligence Optimization and Recurrent Long Short-Term Memory," *Fractal and Fractional*, vol. 7, no. 8, Aug. 2023, Art. no. 598, https://doi.org/10.3390/fractalfract7080598.

[24] A. M. Dayana and W. R. S. Emmanuel, "An enhanced swarm optimization-based deep neural network for diabetic retinopathy classification in fundus images," *Multimedia Tools and Applications*, vol. 81, no. 15, pp. 20611–20642, Jun. 2022, https://doi.org/10.1007/s11042-022-12492-0.

[25] S. Sundaram *et al.*, "Diabetic Retinopathy and Diabetic Macular Edema Detection Using Ensemble Based Convolutional Neural Networks," *Diagnostics*, vol. 13, no. 5, Mar. 2023, Art. no. 1001, https://doi.org/10.3390/diagnostics13051001.

[26] S. Lakhera and A. Garg, "Diabetic Retinopathy Classification Using PSOSVM Based Deep Learning Model," in *2023 Seventh International Conference on Image Information Processing (ICIIP)*, Solan, India, Nov. 2023, pp. 183–187, https://doi.org/10.1109/ICIIP61524.2023.10537630.

[27] O. Higgins and C. Thompson, "Combination of artificial neural network and particle swarm intelligence algorithm for diagnosing diabetes," *Advances in Engineering and Intelligence Systems*, vol. 3, no. 1, Mar. 2024, https://doi.org/10.22034/aeis.2023.427439.1146.

[28] R. G. Tiwari and A. Kumar, "Integrated Transfer Learning and Nature-Inspired Optimization for Enhanced Feature Extraction in Diabetic Retinopathy Image Analysis," in *2024 ASU International Conference in Emerging Technologies for Sustainability and Intelligent Systems (ICETSIS)*, Manama, Bahrain, Jan. 2024, pp. 1–6, https://doi.org/10.1109/ICETSIS61505.2024.10459394.

[29] L. Xiao *et al.*, "HHO optimized support vector machine classifier for traditional Chinese medicine syndrome differentiation of diabetic retinopathy," *International Journal of Ophthalmology*, vol. 17, no. 6, pp. 991–1000, Jun. 2024, https://doi.org/10.18240/ijo.2024.06.02.

[30] V. Sapra *et al.*, "Diabetic Retinopathy Detection Using Deep Learning with Optimized Feature Selection," *Traitement du Signal*, vol. 41, no. 2, pp. 781–790, Apr. 2024, https://doi.org/10.18280/ts.410219.

[31] L. K. Singh, M. Khanna, and R. Singh, "Feature subset selection through nature inspired computing for efficient glaucoma classification from fundus images," *Multimedia Tools and Applications*, vol. 83, no. 32, pp. 77873–77944, Feb. 2024, https://doi.org/10.1007/s11042-024-18624-y.

[32] "National Medical Centre." https://nmc.net.pk/.